NAVIER-STOKES CALCULATIONS AT AEROSPATIALE MATRA AIRBUS FOR AIRCRAFT DESIGN

Cyril GACHERIEU, Ranjit COLLERCANDY, Pascal LARRIEU, Stephane SOUMILLON, Loic TOURRETTE, Stéphane VIALA
Aerospatiale Matra Airbus

Keywords: *Navier-Stokes, preconditioning, ALE, CHT.*

Abstract

This paper describes the present applications of Navier-Stokes solvers at the aerodynamics department of AM Airbus. A large variety of Navier-Stokes simulations are presented. The Navier-Stokes methods are necessary to study complex phenomena for which simpler methods fail or are not sufficiently accurate.

1 General Introduction

Numerical methods are now widely used all along the Aircraft design process. Aerospatiale Matra Airbus (AM Airbus) uses them within the scope of its responsibilities in the Airbus and ATR programs, for the design of aerodynamic shapes and the computation of aerodynamic data for performance and handling qualities, in complement to wind-tunnel tests.

The Euler model with or without boundary layer coupling is mainly employed, due to its relatively low computing costs. Nevertheless, for several design issues, this model is not accurate enough for correctly modeling viscous effects, and Navier-Stokes calculations are required.

To illustrate this point, we propose in this contribution to present the most recent Navier-Stokes simulations performed at AM Airbus to address design issues like :

- qualification of engine installation in severe flight conditions (steep descent), for which separation can occur on a non-optimized pylon. It is fundamental to be able to predict this separation which generates buffeting. An accurate simulation of this phenomena can actually reduce the design cycles. At present we use a simplified method by only simulating the viscous effects on the wing. We first showed that this cost effective method is capable of predicting the birth of separated flows. Then, we showed that the CPU and memory requirements for a full Navier-Stokes simulation could be considerably reduced so that a big computation is now compatible with the AM Airbus design engineer’s constraints.

- evaluation of total pressure distortions at the fan face of the air inlet for the qualification of the air inlet at the fixed point in crosswind.

- decrease the overall design cost, by reducing the number of wind tunnel tests, to fine tune the aircraft flight control laws by introducing progressively in the design stages reliable and accurate CFD tools such as ALE approach for the prediction of flight control derivatives.

- assessment of Reynolds effects for transposition from wind-tunnel to flight,

- optimization of the exhaust of the nacelle anti-icing system, design of the ventilation system of nacelle compartments which require aerothermic coupling. Accurate prediction of thermal environment allows to optimize design and contribute to development cycle reduction.

2 NSMB code

We briefly introduce the present Navier-Stokes code, NSMB, used for all our applications, except for conjugate heat transfer computations which were performed with the Fluent code.

2.1 Space Discretization

A description of the Navier-Stokes solver NSMB for the design of aircraft can be found in [1]. It is the result of collaborative work between aeronautical industries and research centers: AM Airbus , CERFACS (France), EPFL (Switzerland), KTH (Sweden) and SAAB (Sweden). NSMB is written on top of the MEMCOM data base system, and uses a dynamic memory allocation (DMM). It solves the 3D Reynolds-Averaged full Navier-Stokes equations on structured multi-block grids. A cell-centered finite volume approach is used for space discretization of the mean flow equations. The inviscid flux vectors at cell faces are approximated using different schemes, but the majority of the applications are done with the central scheme. Indeed, Jameson's central scheme is cost effective, robust, and gives accurate results if the influence of the artificial dissipation in boundary layers is reduced by scaling the wall normal artificial dissipation fluxes with a function of the local Mach number [2].

2.2 Time integration

Simulations over complex geometries are highly CPU demanding because of the large number of grid points. Highly stretched cells in the viscous region and turbulence models require a robust algorithm to obtain convergence. Therefore, the LU-SGS [3] (Lower-Upper Symmetric Gauss-Seidel) method has been implemented in NSMB. This scheme combines a low computing cost with a reasonable convergence rate. In addition, the scheme has a low memory requirement which is important for the computation of complex geometries. The algorithm has been adapted for efficient computations using parallel computers [4]. The inversion of the linear system is done by forward and backward Gauss-Seidel sweeps across the computation domain. An update of the block interface boundary conditions between the sweeps allows the convergence to be independent of the block decomposition of the computation domain. The LU-SGS method does not exhibit any time step restriction and CFL numbers up to infinity are used for the computations. Moreover, in comparison with explicit schemes, the LU-SGS method accepts smaller values of the fourth order artificial dissipation coefficient , thus improving the accuracy of the solutions.

In order to avoid block matrix inversions, approximations using spectral radii of the jacobian matrices are applied to the LU factors. This simplification, for which we call this algorithm LU-SGS "scalar", downgrades the convergence rate for highly stretched meshes. A more accurate method, LU-SGS "matrix" overcomes this weakness of the LU-SGS. Unfortunately the associated memory requirement became too large for industrial configurations on our present computer. So we focus FAS multigrid [5] with the LU-SGS used as a smoother since it improves the LU-SGS "scalar" performance without significant increase of the memory requirement.

2.3 Turbulence modelling

In priority, we looked for a robust and cost effective turbulence model suitable for complex geometries and multi-block meshes. A considerable effort has been invested at AM Airbus in the definition of a genuinely multi-block implementation of the algebraic turbulence models which makes them independent of the domain decomposition [2]. To overcome the limitations of the algebraic models, we encourage the use of a turbulence model equation. Among all the turbulence models available in NSMB, for the time being we selected the Spalart-Allmaras (SA) [6] turbulence model because of its reasonable results on a wide range of flows and its good numerical properties. The mean flow field and the turbulent equation are decoupled at each time step. The implicit operator is constructed according to [6] so that a positive turbulence field is obtained for all transient solution states.

3 Aircraft Applications

3.1 Euler-NS aircraft applications

The application of the Navier-Stokes methods in an industrial context depends on:

1) The ability to simulate separate flows for which weak coupling codes fail.

2) moderate CPU and memory requirements. Our present computer is a CRAY (20 sv1 processors, a peak node speed: 1Gflops, memory: 2Gw).

To meet these 2 criteria, AM Airbus tested a "mixed" viscous-inviscid computation strategy.

The most sensitive separations mainly appear on the lifting surfaces. So, as a first step, it is reasonable only to simulate viscous effects on the wing. For example, with an original Euler mesh of body, nacelle, wing and pylon configuration containing 1 million nodes, the "mixed" mesh only needs 1,5 million nodes because it is only refined around the wing. In comparison the equivalent full Navier-Stokes mesh would contain 5 millions nodes. This significant decrease in mesh size permits moderate memory and CPU requirements.

The present study focuses on 2 different aerodynamic conditions which often lead to separate flows:

a) High Mach and low Cl for a four engine aircraft configuration (on the pressure side, inboard side of the outboard pylon).

b) High Mach and high Cl (classic separation on the upper side).

For case a), "Mixed" computations were done on a 4 engine configuration making it possible to predict separation at the leading edge on the inboard side of the outboard engine (O/B pylon I/B side) (Fig. 3.1 and Fig. 3.2). This computation, done with 2 multigrid levels, was obtained after 6 hours on 4 processors and needed 211Mw. When the Cl decreases, a separation bubble at the root of the shock appears (Fig. 3.1). This bubble is well simulated on the skin friction lines (Fig. 3.2). For a lower Cl, the bubble bursts and the shock disappears. This phenomenon was already observed experimentally for similar aerodynamic conditions. So, despite the numerical slip condition applied to the pylon, the simulated separations are sufficiently representative of the real flow. However, if the bubble extends, the difference between computed pressure distributions and experimental data increases. It is obvious that if the separation spreads, then the simulation of the viscous effects on the pylon becomes necessary. Moreover, the steady approach is no longer appropriate if the separation has a greater extent and a higher intensity.

The "mixed" computations were also applied to predict the separation which appears on the upper side of the wing for high Mach and Cl, Fig. 3.3. These computations were not accessible to weak coupling methods. For a body, wing, winglet, pylon and nacelle configuration, only 2.7 million nodes were necessary, and the solution is obtained after less than 10 hours on 4 processors (2 multigrid levels) and requires 290Mw.

3.2 Full NS aircraft application

To improve the prediction of the flow field in the vicinity of the pylons, we tested the capacity of NSMB to solve an aircraft configuration with all the walls defined as Navier-Stokes walls. Refining all the boundary layers of complex geometries makes the mesh generation more difficult. Due to structured topology and C topology around each element, the number of nodes tends to increase a lot. So a compromise is needed between a good general mesh quality and an acceptable total number of cells. The 3 multigrid levels impose a minimum of 8 cells in each mesh line direction, so the multigrid slightly contributes to increasing the amount of mesh points. It is also well known that this acceleration method is sensitive to mesh quality. In particular, we observed its inefficiency when too large differences of cell size appeared at block interfaces. Nevertheless, multigrid is a necessity to converge such large configurations over night. It is a pity not to use it on a very big mesh because of a minority of incorrect cells. We recently worked on the development of corrections to make the multigrid more robust on these "bad" meshes. These corrections greatly improved multigrid robustness.

To illustrate the performance of NSMB, we selected an Aircraft configuration Fig. 3.1 which represents all the characteristics met in engine integration: The inboard nacelle is a TFN (through flow nacelle) and the outboard nacelle is a TPS (Turbo powered simulator). The finest mesh contains about 9.5 million nodes spread over 107 blocks. The cruise conditions correspond to Re/m=12 millions, α=2.616° and M=0.82. For this big configuration, we used 8 CRAY sv1 processors.

This application confirms the advantages of the multigrid method: For approximately 12% increase in memory requirement tab[1], an impressive improvement in the convergence rate is obtained, Fig. 3.5 and Fig. 3.6.

8 procs	Memory (Mw)	CPU (s/i)
1g	847	46.7
2g	938	81.7
3g	956	83.3

Tab. 1: Memory and CPU consumption with 8 CRAY sv1 processors for 9.5 10^6 nodes

Fig. 3.6 also confirms the advantage of working with 3 grid level meshes. In comparison with the 2 grid level, the third grid level offers significant convergence benefits for a very small additional cost. Indeed, despite its size, its complexity and the moderate performance of our computer, this configuration is converged before 7 elapsed time hours.

Fig. 3.8 to 3.10 show the pressure coefficient distribution for 3 sections near the 2 pylons (defined in Fig. 3.7). The comparison with experimental measurements is quite good. The biggest difference appears for section 2700, Fig. 3.9, at the pressure side, near the leading edge, where the second small shock is underestimated. The reason is that a close flap track fairing (FTF) has not been simulated yet. The latest NSMB version accepts patched grid interfaces. So to have access to a more accurate simulation, we will be able to add this FTF without increasing the mesh size.

3.3 Conclusions and perspectives

The NSMB Navier-Stokes solver is already enough robust and cost effective to give access to precious Navier-Stokes solutions on full aircraft configurations respecting our industrial constraints. The latest improvements in NSMB will contribute to offer a better accuracy.

4 Air-intake calculations in cross-flow wind

4.1 Introduction

The motivation is to provide nacelle designers with a reliable numerical tool for the prediction of stagnation pressure distortions at the fan face as a function of the mass flow rate, in cross-flow wind, when the airplane is on the ground, before take-off, and especially the divergence point, that appears for sufficiently high mass flow rates.

The main difficulties in this type of computation are:

- coexistence of two radically different types of flow: very low Mach number flow ($M_\infty \approx 0.045$) outside, transonic flow inside,
- strong accelerations at the leading edge, due to the high value of the side-slip angle, followed by strong shocks which may induce boundary layer separation,
- need for a boundary condition allowing a rigorous prescription of the desired global mass flow rate through the fan face.

The very low speed regions of the flow are taken into account through the use of a local preconditioning method ([1-3]) which addresses the well-known problems of convergence and accuracy affecting the compressible codes in the limit $M\infty \to 0$.

A strict control of the global mass flow rate is ensured by a boundary condition adapted to internal viscous flows, specially developed for this study.

4.2 Description of test-cases

The aerodynamic conditions are given below:

$M_\infty=0.045$, $\alpha=0°$, $\beta=90°$, Reynolds number per unit length $Re_1=3.78\ 10^6\ m^{-1}$

Five calculations were performed, corresponding to the values W_R=*800, 900, 1000, 1020* and *1040 lbs/s* of the “reduced” mass flow rate, using the Baldwin-Lomax turbulence model.

4.3 Grid

The Navier-Stokes mesh is made of 10 structured blocks with 968682 nodes and 3 levels of grid. The boundary layer was adapted to the internal flow (using a unit Reynolds number based on the mean value of the Mach number in the fan face) with about 25 points along the normal direction and a y^+ value of 2 at the center of the cells adjacent to the wall. The spinner is treated as an inviscid wall and the fan face was shifted downstream at a distance from the leading edge equal of approximately three times that of the "real" fan face.

4.4 Results

In the majority of compressible codes, the equations are made non dimensional using the free stream speed of sound as a reference velocity. In the limit $M_\infty \to 0$, the asymptotic behavior of the equations shows that it becomes rapidly impossible to use them as a mean of updating the pressure. The fundamental idea behind preconditioning consists in replacing the *global* reference velocity c_∞ by the *local* flow speed V.

The state-of-the-art in local preconditioning for the Navier-Stokes equations includes the following ingredients:

- replacement of the local velocity by $min(V, ConstV_\infty)$, $Const=O(1)$, to avoid problems in the vicinity of stagnation points ([1]),
- use of a velocity scale V_{pgr} based on the pressure gradient to enhance robustness ([3]),
- use of a viscous velocity scale in low Reynolds number regions ([2]),
- high cell-aspect-ratio preconditioning ([2]).

These perform quite well in the inviscid case but prove to be insufficient for viscous simulations for which specific improvements were necessary.

The calculation of a given mass flow rate requires about 1000 multigrid cycles, i.e. an elapsed time of approximately 4500 s CPU on 4 CRAY sv1 processors, with a maximum memory of 118 Mwords used.

Fig. 4.1 shows the isentropic Mach numbers on the nacelle. The free stream velocity vector is parallel to the y-axis and directed towards the positive y values.

Fig. 4.2 compares the computed and experimental isentropic Mach number distributions in the plane at θ=90°, side y<0 (see Fig. 4.1). The suction peak is well predicted, indicating that the level of artificial dissipation is sufficiently low at the leading edge. At the position of the "real" fan face ($x=0.208$), the flow is slightly too rapid, due to an overestimated boundary layer height. This is confirmed by the stagnation pressure profile at $\theta=90°$ in the fan face (Fig. 4.3). Finally, Fig. 4.4 represents the level of stagnation pressure distortion in the fan face as a function of the mass flow rate. For moderate mass flow rates ($W_R=800$, 900), the level of distortion is predicted too high. It is estimated much better at $W_R=1020$, 1040. In the experiment, the divergence occurs around $W_R=960$ whereas in the computation, it happens slightly later, between $W_R=1000$ and $W_R=1020$.

4.5 Conclusions and perspectives

The compressible Navier-Stokes equations can be successfully applied to simulate air-intakes in cross-flow wind. The low computation cost together with the accuracy of the numerical results make it a promising tool for designing nacelles. In order to improve the representation of the boundary layer as well as the overall accuracy of the numerical solution, more validation is currently under way on new geometries using more advanced turbulence models (e.g. Spalart-Allmaras one-equation model) and numerical schemes (second order upwind schemes), with already very promising results.

5 ALE approach – Aircraft Stability Derivatives

5.1 Introduction

The stability derivatives of the aerodynamic forces are essential for the airplane manufacturers in order to fine tune the control laws and to ensure the stability of the aircraft. The classic method of determining the control derivatives, constructing and testing wind-tunnel models, is expensive and requires a long lead time for the resulting data. Even though most of the previous numerical work is still based on semi-empirical methods and other simplified inviscid theories, the recent trend is to use the turbulent Navier-Stokes prediction capabilities for their computations. Such studies have been recently undertaken at AM Airbus using the ALE (Arbitrary-Lagrangian-Eulerian) technique available in the NSMB code to study the rotating effects on the airplane due to the rolling velocity p, pitching velocity q and yawing velocity r [10].

5.2 Computation test case and Results

This part of the paper concerns one of the applications of this technique for the simulation of steady longitudinal dynamic derivatives of an aircraft configuration. Thus the airplane is rotating with a pitching velocity q about an axis through the center of gravity normal to the plane of symmetry. All computations are done using Jameson's centered scheme coupled with a scalar LU-SGS multigrid implicit time stepping scheme. The turbulent effects are modeled using the Spalart-Allmaras one-equation model.

The test case is a civil aircraft configuration composed of fuselage, wing and winglets , and with horizontal and vertical tail-planes. A multi-block structured mesh consisting of 48 computation blocks and around 3 million points, for the half configuration, is used for the present study. Further, three grid levels are also used in all the computations. The numerical simulation corresponds to a free stream Mach number of 0.22 and a Reynolds number per unit meter of 4.74 10^6. In order to estimate the different derivatives, standard computations without the ALE approach at two relatively close but finite values of the angle of attack α are initially carried out to determine the corresponding static lift and moment derivatives $C_{L\alpha}$ and $C_{M\alpha}$. Next the dynamic lift and moment derivatives, C_{Lq} and C_{Mq}, are determined from a ALE computation for a chosen value of the angle α and for a normalised pitching velocity q^* which is taken here to be 0.005. These coefficients are then obtained from finite difference approximations corresponding to the values of α or q^*. A partial view of the computation mesh along with the pressure coefficient distribution, for q^* corresponding to 0.005, is presented in Fig. 5.1.

The preliminary results for the steady dynamic derivatives obtained using the NSMB code shows fairly good agreement with the available experimental data.

5.3 Conclusions and perspectives

The Navier-Stokes equations using the ALE formulation are successfully applied to the computation of stability derivatives of a complex aircraft configuration. The results obtained demonstrate the potential perspective of numerical techniques for the aircraft stability study. Using Navier-Stokes solvers, it is now possible to analyze the local flow phenomena which were not accessible with semi-empirical formulations. Studies are also under way to include unsteady characteristics such as the time variation of the effective angle of attack $\dot{\alpha}$ in the computations. Further, calculations are now being performed at AM Airbus to validate the rolling and yawing contributions around complex aircraft configurations as well.

6 Reynolds number effect

6.1 Introduction

Wind-tunnel tests are a good way to study all the phenomena on an aircraft model. Unfortunately, in general they are not completely representative of the flight conditions because of the low Reynolds number obtained in tunnel tests.

Some comparisons between flight and tunnel tests have shown that the effect of Reynolds number may sometimes be the cause of an unexpected aircraft behavior in flight. This effect is strongly dependent on the flow around the aircraft and therefore on the geometry and the flight conditions. So this effect is very difficult to predict from one aircraft to another.

Therefore, it is important for aircraft manufacturers to assess the Reynolds effect before first flight. The use of CFD is a suitable way of carrying out this prediction because it allows to handle easily and at low cost various configurations, flight conditions and Reynolds numbers.

6.2 Test cases

Two test cases are presented to illustrate these phenomena.

The first one is a complete Wing/Body/Winglet Navier-Stokes structured mesh of 2.5 millions points. The Reynolds numbers are 4.2 and 68 million and the flow conditions are a Mach number of 0.85 and an angle of attack of 1.5 giving a small lift coefficient (≈0.35).

The second one is a partial Navier-Stokes (only on the wing) Wing/Body configuration of 800000 points. The low number of mesh nodes allows a polar of several flight points to be computed during the night for a good prediction of Reynolds effect on the wing. The Reynolds number is 4.2 and 50 million for tunnel and flight conditions. The Mach number is 0.82 and the angle of attack varies between 0. and 3.0 degrees.

6.3 Results and comments

Fig. 6.1 and 6.2 show the typical effect of Reynolds number on the pressure coefficient distribution on the wing for the two test cases. The passage from low to high Reynolds number causes a diminution of the boundary layer thickness which causes the shock to move toward the trailing edge and increase its strength. As explained in the first part of this paper, this effect is strongly dependent on the configuration and the flight condition used. Fig. 6.3 and 6.4 show the effect of Reynolds number on the second configuration for angles of attack of 1.0 and 2.0 degrees.

The analysis of the drag coefficient obtained through farfield analysis for many angles of attack give the polar at Mach=0.82 shown in Fig. 6.5. The difference in behavior for the two Reynolds numbers can be seen. This drag polar shape can be used to correct the wind tunnel data obtained for the aircraft model. Also, these results can be used for tunnel to flight scaling methodologies on the whole aircraft.

6.4 Conclusions

The numerical simulation at any Reynolds number and any flight condition allows good characterization of the Reynolds effect for simple or complex configurations. This simulation allows CFD drag coefficients results to be included in the design process of transport aircraft through the assessment of aircraft performance in flight conditions.

7 Conjugate heat transfer computations

The use of carbon fiber composite (CFC) is becoming increasingly widespread in aircraft construction due to the benefits associated with its high strength to weight ratio. However, the reduction in material strength properties at high temperature means that one has to take care about the surrounding thermal environment and to optimize thermal design.

7.1 Methods

Depending on the complexity of the thermal model AM Airbus uses two conjugate heat transfer (CHT) methods.

7.1.1 Simple thermal model

Problems ranging from thermal mixing within a fluid to conduction solids in quite simple geometry are handled using FLUENT V5 [1]. This CFD code allows us to include heat transfer within the fluid and/or solid regions.

This tool has been validated on the nacelle anti-ice (NAI) exhaust outlet for which dynamic phenomena are dominant. The CFD model of the exhaust arrangement consists of an exhaust outlet located in a flat plate representing the external surface of the nacelle (Fig. 7.1). The local flow conditions at the exhaust flow velocity and local external velocity were properly represented. A full potential code developed by AM Airbus was used on a model of an isolated nacelle for calculation of local external CP's from which the local flow conditions were established as an input to FLUENT V5.

Adiabatic wall temperature predictions are shown on Fig. 7.2. They are in good agreement with flight test measurements. Turbulence models with the Boussinesq assumption seem to have little effect on thermal results.

7.1.2 Complex thermal model

The integrated CHT method described above is not very suitable for complex geometry and/or complex thermal models. In these cases, the thermal conduction and radiation are solved using TMG or NASTRAN solver while the fluid domain is computed using FLUENT V5. A coupling method for fluid and thermic solvers, working most of the time on non-matching grids has been developed. This allows independent engineers or teams to generate solid and fluid meshes on a common geometry.

Here, the coupling is obtained via exchange of boundary conditions (b.c.). The fluid solution is obtained with a predicted temperature distribution along coupled walls; the heat flux computed by the FLUENT solver (explicit contribution) and the turbulent heat exchange coefficient, noted *h*, associated with a reference temperature (implicit contribution) are then used as b.c. for the thermal solver, which gives a new temperature distribution along the walls. The *h* coefficient is determined using a turbulent wall function associated with the Reynolds analogy.

The use of a heat flux b.c. for the solid and a temperature b.c. for the fluid ensures stability of the global problem according to Giles [12], while a Neumann condition for the fluid and Dirichlet for the solid may lead to instabilities.

The interpolation procedure determines which elements and nodes of the other boundary mesh should be retained and the weight to apply for interpolation. This is done once, and all transfer information is stored. Then the data transfer from one grid to the other is performed at very low cost.

This coupling process has been validated on simple cases (not detailed in this paper). The results presented below are preliminary and a large validation campaign is in progress. Fig. 7.3 shows a 3D validation case where the CHT process described above provides some relevant information which is difficult to predict with an individual engineer's skill. The thermal model solved by TMG is summarized on Table 7.1. The mass flow inlet condition is 0,8 Kg/s at 343 K and the jet mass flow inlet condition is 12 g/s at 333 K.

	Material	Width	Thermal condition
Upper wall	*Aluminum*	*1 mm*	*800 W/m^2*
Lower wall	*Steel*	*1 mm*	*Adiabatic*
Outlet wall	*Orthotropic CFC*	*1 cm*	*h=5W/m^2/K T=353K*
Right wall	*Isotropic CFC*	*2 cm*	*h=14W/m^2/K T=323K*
Back wall	*Steel*	*2 cm*	*h=5W/m^2/K T=353K*
Tube	*Steel*	*1 mm*	*h=1000W/m^2/K T=333K*

Table 7.1: Thermal model

Heat transfer modifications due to recirculating and impinging jet are significant in such configurations (Fig. 7.3). They are not easy to predict with empirical correlations. Convergence of the coupling process (every 10 fluid iterations here) is plotted on Fig. 7.4.

7.2 Applications

7.2.1 Nacelle anti-ice exhaust outlet design

As the NAI spent air mixes with ambient air, the exhaust plume will tend to re-attach to the nacelle surface, particularly during climb flight conditions. Since it is possible for the NAI exhaust air to be relatively hot, there may arise a concern about increased temperatures at the re-attached exhaust plume. This could overheat CFC structure so it is desirable to design an NAI exhaust outlet which minimize wall temperature downstream.

The arrangement used for design process has been described in paragraph 7.1.1. Relevant parameters are :

The outlet open area : reducing the exhaust outlet area may increase the exhaust velocity and promote a longer cooling of the exhaust plume before it is re-attached. The constraints on this approach are structural (maximum allowable D-chamber pressure) and thermal (NAI system performance decreases with pressure).

Sub-division of flow : division of the exhaust outlet area into a number of smaller separate areas may improve thermal mixing.

Outlet and outlet edge geometries may have a great influence on the plume re-attachment point, mixing process and location of re-attachment.

Noise generation : Flows over open cavities are a significant source of noise. Unfortunately, CFD could not be used to quantify noise levels generated by complex exhaust outlet configurations.

Cross flow effects : Local cross flow effects (tilting of the exhaust centerline with respect to local external flow direction) may reduce mixing performances.

All these requirements must be considered for the design process. Fig. 7.6 shows the model and results on a particular NAI outlet configuration. Thermal mixing and conduction in solids are performed with FLUENT V5. Skin friction lines colored by temperature results show how the sub-division of flow allows free stream air to flow between separate exhaust plumes. This improves mixing and creates a larger exhaust plume surface area in contact with the cooler air.

7.2.2 Air conditioning compartment ventilation

In order to check temperature on the CFC component which is located in the air conditioning compartment, a CHT computation has to be performed. As the geometry and thermal phenomena are complex the method described in paragraph 7.1.2 was used with NASTRAN as a thermal solver.

Fig. 7.5 shows the results. Such computations provide information on jets and global cooling effects. Thermal optimization of the system locations can then be dealt with.

8 General conclusion and Perspectives

Navier-Stokes simulations are more and more employed at AM Airbus to address design issues in various domains: design of aerodynamic shapes, assessment of performance and handling quality, ventilation studies. We have presented the most recent Navier-Stokes applications. Due to recent improvements in efficiency, we can get rid of the limitations inherent to simpler modelisations and thus access to more complex physical phenomena at reasonable cost and delay. We are going to use patched grids, adaptative mesh refinement (AMR) and more complex turbulence models. With such improvements, Navier-Stokes methods will be more and more easy to use and will be integrated in numerical optimization tools. The Navier-Stokes method will significantly contribute to reduce the cost of design cycles.

References

[1] Vos JB, Rizzi AW, Corjon A, Chaput E, Soinne E. *Recent advances in aerodynamics inside the NSMB (Navier-Stokes multi-block) consortium*, AIAA-paper 98-0225.

[2] Chaput E, Barrera L, Gacherieu C, Tourette L. Navier-Stokes *analysis for engine airframe integration*. ICAS, Sorrento, 1996.

[3] Yoon S, Jameson A, *A multigrid LU-SSOR scheme for approximate newton iteration applied to the euler equations*, NASA-CR-179524, 1986.

[4] Weber C, *Parallel implicit computations of turbulence transonic flow around a complete aircraft configuration*, ParallelCFD97, Manchester, 1986.

[5] Hackbusch W, *Multigrid methods and applications*, Springer-Verlag, Berlin, Heidelberg, 1985.

[6] Spalart PR, Allmaras SR, *A one-equation turbulence model for aerodynamic flows*, AIAA-paper 92-0439, 1992.

[7] Radespiel R., Türkel E., *Preconditioning Methods for Multidimensional Aerodynamics*, 27th CFD Lecture *Series*, Von Karman Institute, VKI-LS1996-06, 1996.

[8] Venkateswaran S., Merkle L., *Analysis of Preconditioning methods for the Euler and Navier-Stokes Equations*, 30th CFD Lecture Series, Von Karman Institute, VKI-LS1999-03, 1999.

[9] Darmofal D.L., Van Leer L., *Multigrid Acceleration of the Preconditioned Euler and Navier-Stokes Equations*, 30th CFD Lecture Series, Von Karman Institute, VKI-LS1999-03, 1999.

[10] Cormier J., Champagneux S., Moreux V., Collercandy R., *Prediction of Quasi-Stationary aerodynamics coefficients using the ALE Method*, ECCOMAS CFD 2000, Barcelone, Sept 2000 (To appear).

[11] *FLUENT 5 User's Guide*. 1st edition, Fluent Inc., 1998.

[12] Giles M. B. *Stability Analysis of Numerical Interface Conditions in Fluid-Structure Thermal Analysis*. International Journal for Numerical Methods in Fluids, Vol. 25, pp 421-436, 1997.

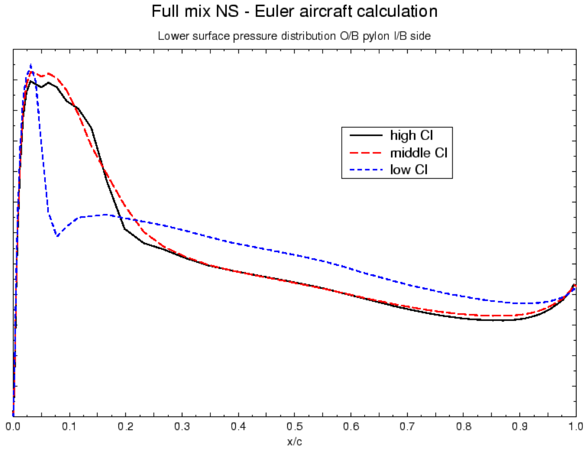

Fig 3.1: Pressure coefficient on O/B pylon I/B side.

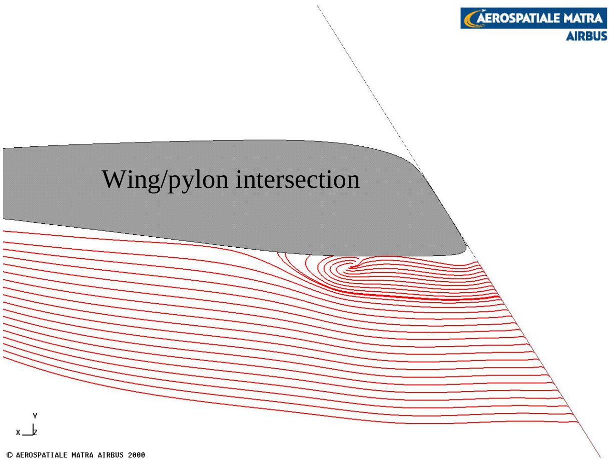

Fig 3.2: Skin friction lines on O/B pylon I/B side.

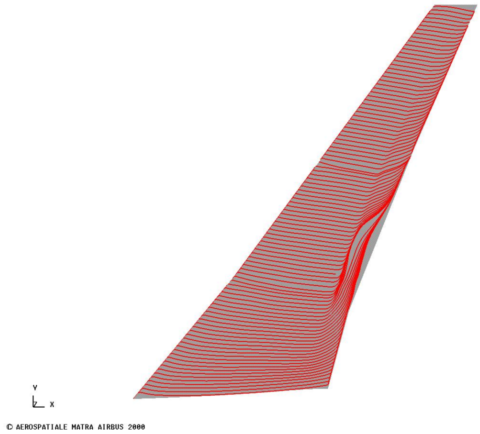

Fig 3.3: Skin friction lines on the upper side.

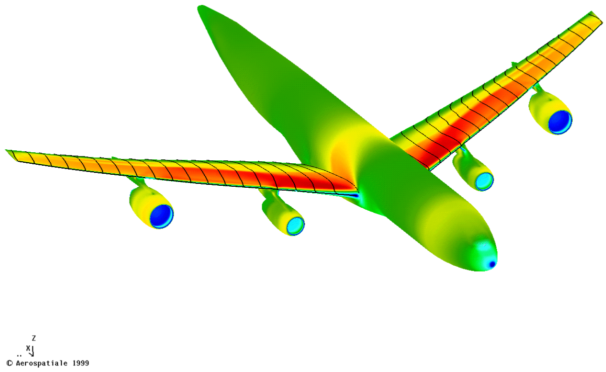

Fig. 3.4 : Pressure field and skin friction lines on full NS Aircraft

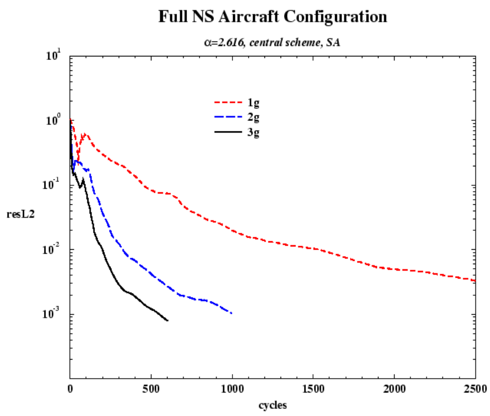

Fig. 3.5: Residual convergence history

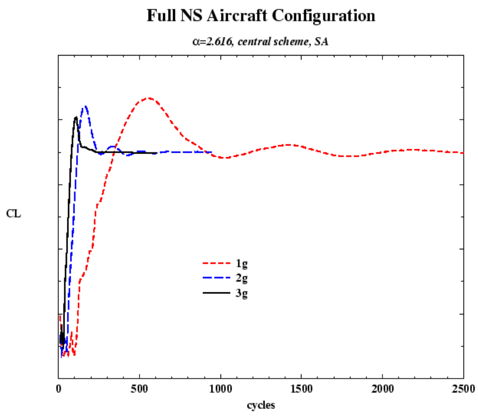

Fig 3.6: Clift convergence history

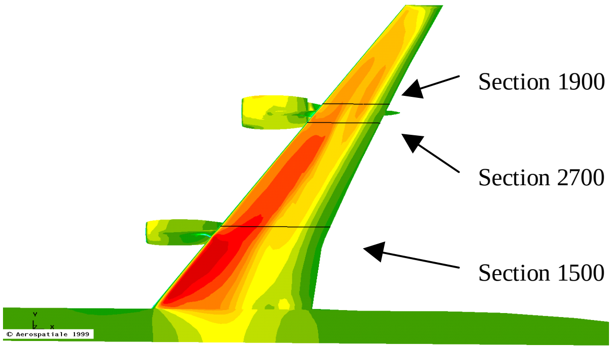

Fig. 3.7: Section location

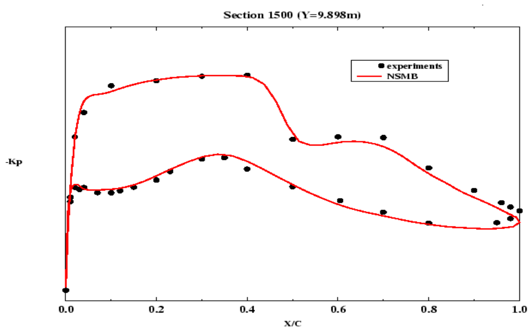

Fig 3.8: Pressure distribution on section 1500

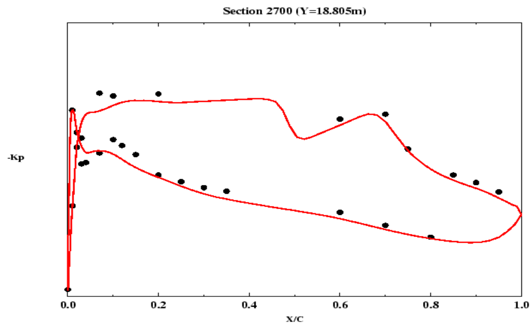

Fig. 3.9: Pressure distribution on section 2700

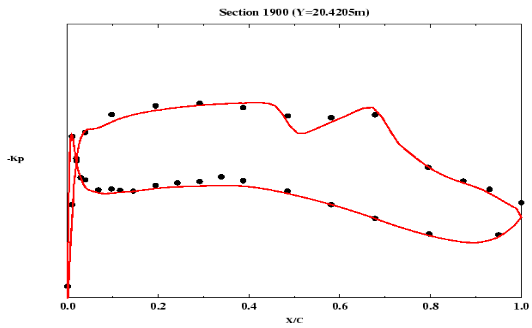

Fig. 3.10: Pressure distribution on section 1900

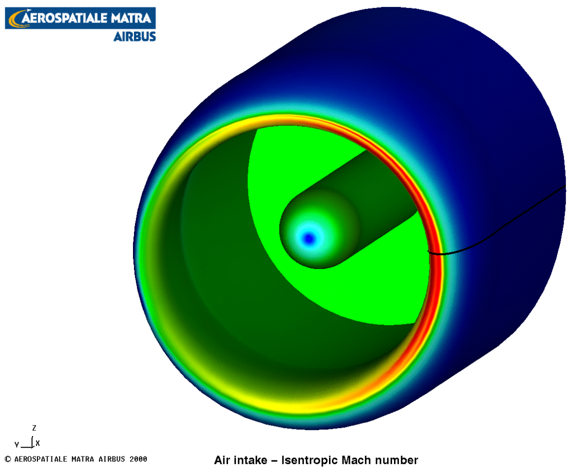

Fig 4.1: Isentropic Mach number field

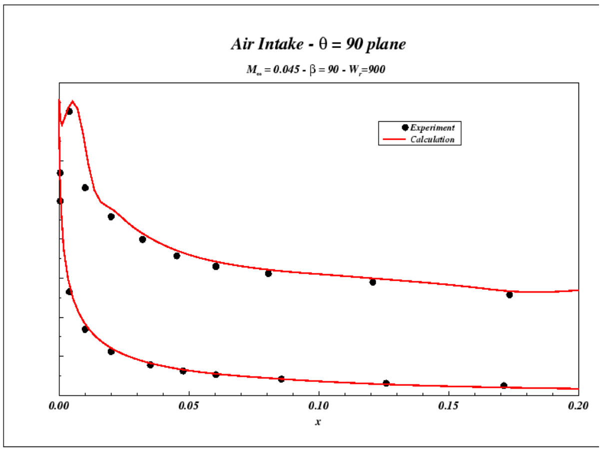

Fig. 4.2: Isentropic Mach number distribution

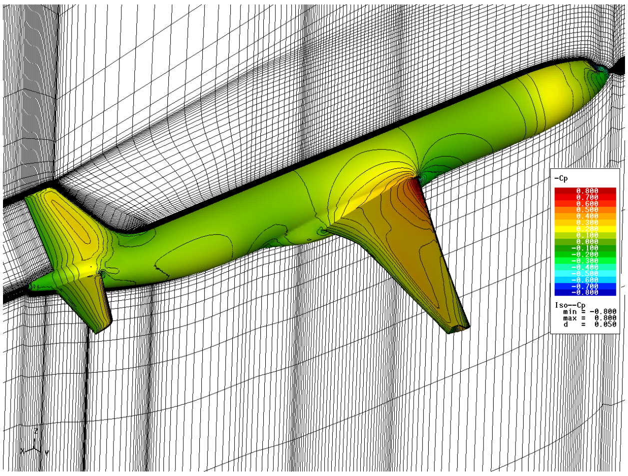

Fig. 5.1: Pressure coefficient distribution for q*=0.005

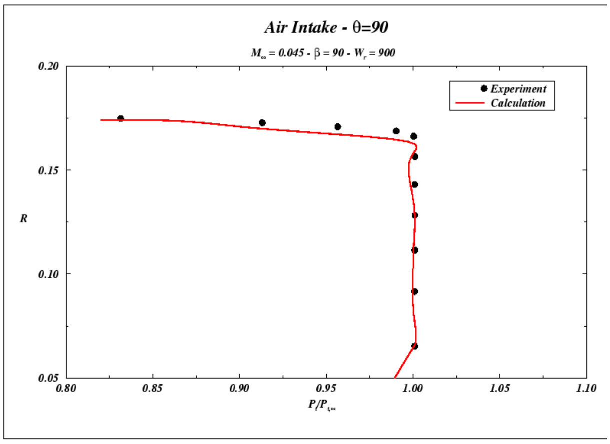

Fig. 4.3: Stagnation pressure profile

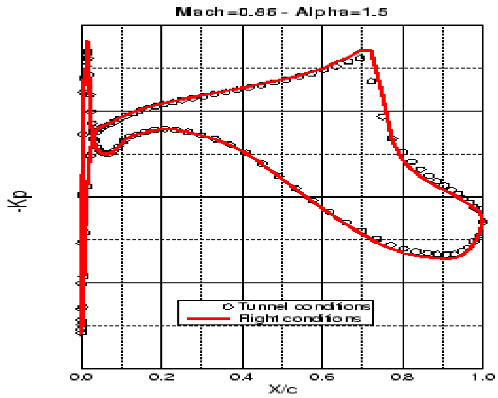

Fig. 6.1: Pressure coefficient (Mach=.85, a=1.5°)

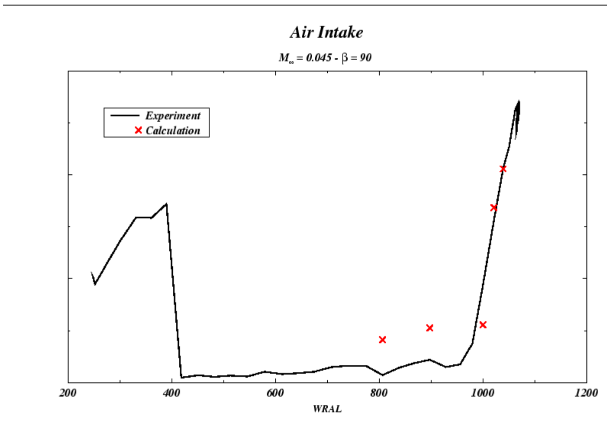

Fig 4.4: Stagnation pressure distortion in the fan face

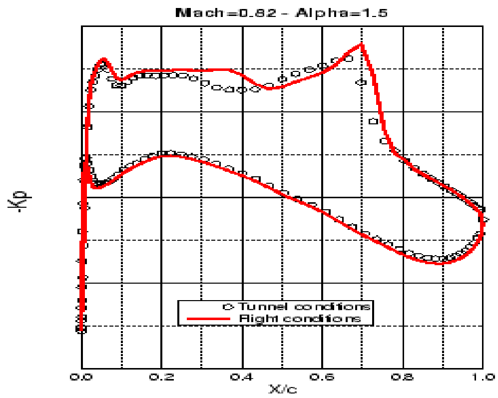

Fig. 6.2: Pressure coefficient (Mach=.82, a=1.5°)

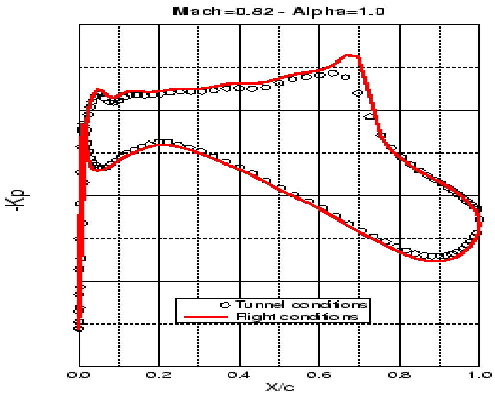

Fig. 6.3: Pressure coefficient (Mach=.82, a=1.0°)

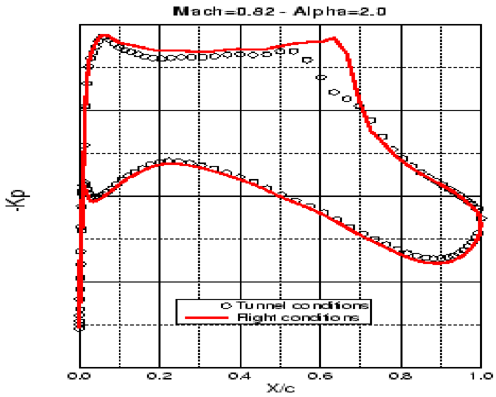

Fig. 6.4: Pressure coefficient (Mach=.82, a=2.0°)

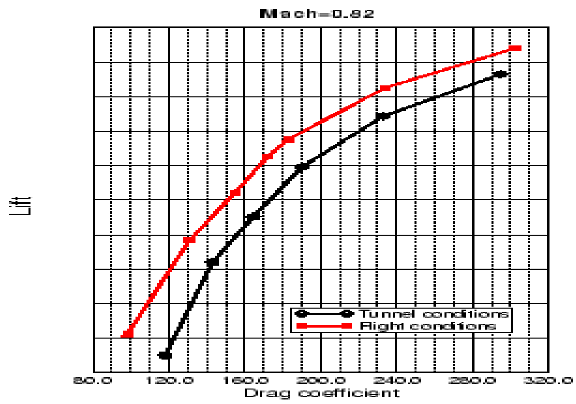

Fig. 6.5: Polar for Mach=.82

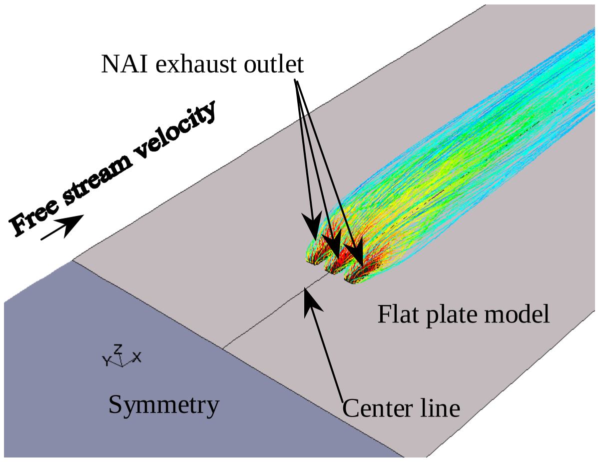

Fig. 7.1: NAI exhaust model - Path line colored by temperature

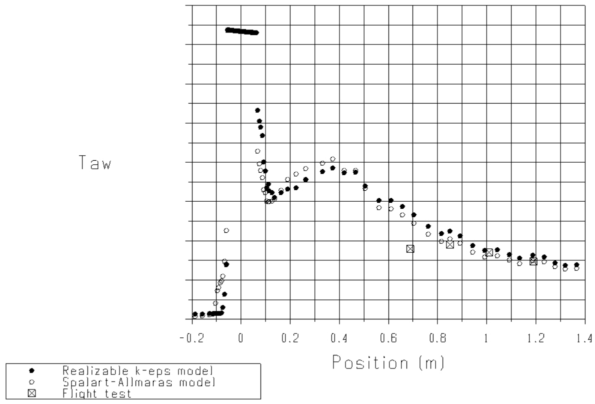

Fig. 7.2 : Adiabatic wall temperature prediction compared to flight test measurement on the center line

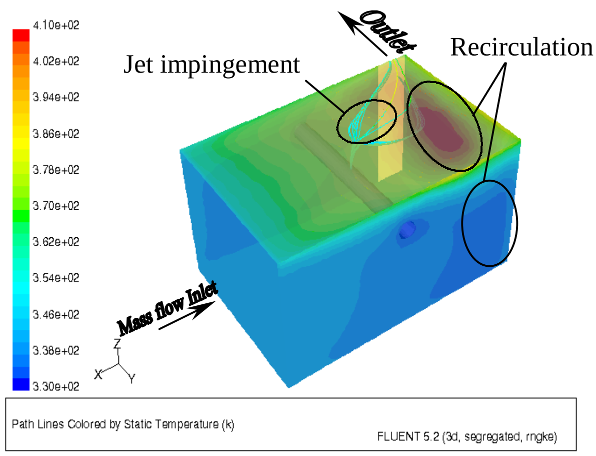

Fig. 7.3 : CHT validation on 3D box with jet impingement - Wall temperature - Jet path-lines colored by temperature

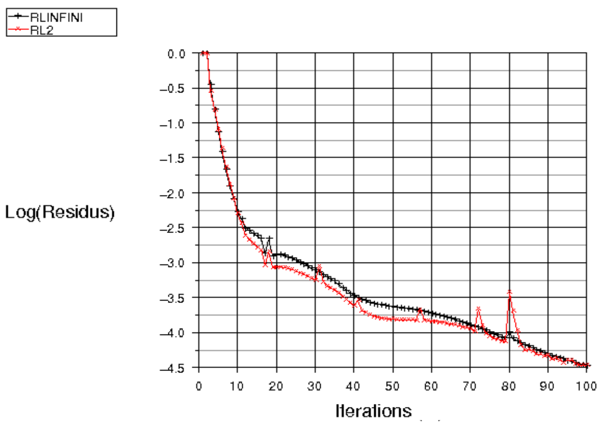

Fig. 7.4 : Convergence of the CHT process - coupled every 10 fluid iterations

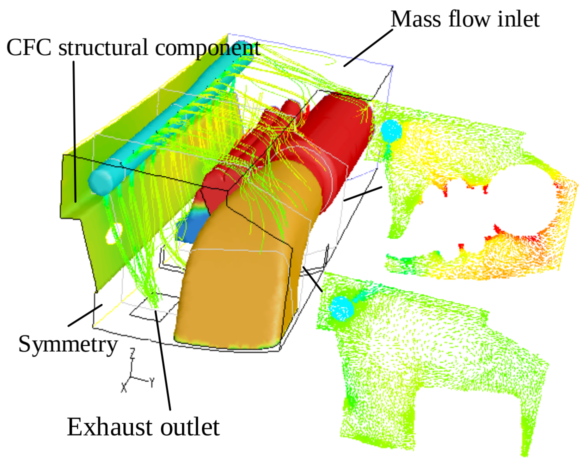

Fig. 7.5 : CFC component cooling application - Wall temperature - Jets path lines colored by temperature - Velocity vectors in plane cuts colored by temperature

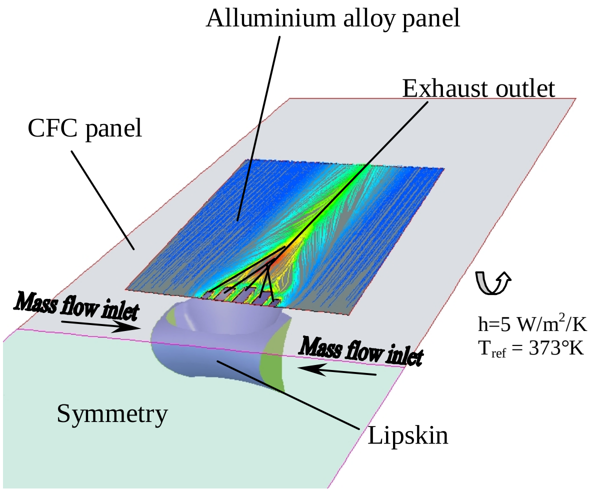

Fig. 7.6 : NAI outlet exhaust design application